
DepthVanish: Optimizing Adversarial Interval Structures for Stereo-Depth-Invisible Patches

Yun Xing^{1,3} * Yue Cao^{1,2} Nhat Chung^{1,7*} Jie Zhang¹ Ivor Tsang^{1,2}
 Ming-Ming Cheng^{4,5} Yang Liu² Lei Ma^{3,6} Qing Guo^{1†}

¹ CFAR and IHPC, Agency for Science, Technology and Research (A*STAR), Singapore

² Nanyang Technological University, Singapore ³ University of Alberta, Canada

⁴ VCIP, CS, Nankai University ⁵ NKIARI, Shenzhen Futian

⁶ The University of Tokyo, Japan ⁷ VNU-HCM, Vietnam

Abstract

Stereo Depth estimation is a critical task in autonomous driving and robotics, where inaccuracies (such as misidentifying nearby objects as distant) can lead to dangerous situations. Adversarial attacks against stereo depth estimation can help reveal vulnerabilities before deployment. Previous work has shown that repeating optimized textures can effectively mislead stereo depth estimation in digital settings. However, our research reveals that these naively repeated texture structures perform poorly in physical-world implementations, *i.e.*, when deployed as patches, limiting their practical utility for testing stereo depth estimation systems. In this work, for the first time, we discover that introducing regular intervals between repeated textures, creating a striped structure, significantly enhances the patch attack effectiveness. Through extensive experimentation, we analyze how variations of this novel structure influence the performance. Based on these insights, we develop a novel stereo depth attack that jointly optimizes both the striped structure and texture elements. Our generated adversarial patches can be inserted into any scenes and successfully attack state-of-the-art stereo depth estimation methods, *i.e.*, RAFTS-tereo and STTR. Most critically, our patch can also attack commercial RGB-D cameras (Intel RealSense) in real-world conditions, demonstrating their practical relevance for security assessment of stereo systems.

1 Introduction

Depth estimation is a critical component in safety-critical embodied systems like autonomous driving [6] and robotics [3], where accurate perception of the 3D environment is essential for reliable operation. Investigating the errors in depth estimation—such as mistaking nearby objects for distant ones in safety-critical embodied systems [28, 5, 35, 8, 18, 39, 38]—can provide critical insights for safety practice. Most existing work focuses on the security vulnerabilities of monocular depth estimation, which relies heavily on scene priors from single images. Stereo depth estimation, on the other hand, utilizes geometric constraints and typically provides more robust and metrically accurate results, making it attractive for high-stakes applications.

However, despite this inherent advantage, recent studies revealed that DNN-based stereo pipelines remain vulnerable to adversarial attacks, as carefully crafted pixel-level perturbations [29, 1] can cause substantial disparity estimation errors. Nevertheless, previous research has primarily addressed digital attacks utilizing full-image noise, which are impractical in real-world contexts due to constraints

*Work done during internship at CFAR & IHPC, A*STAR. †Co-corresponding author, email address: tsingqguo@ieee.org.

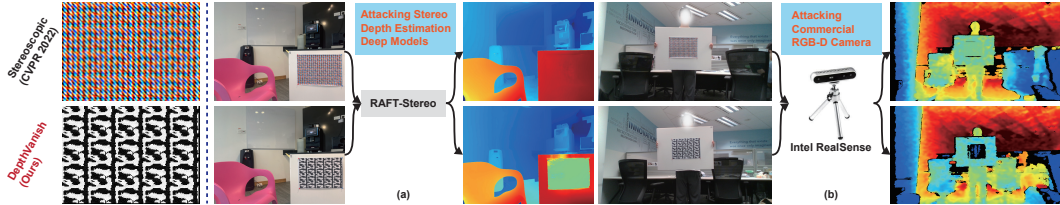


Figure 1: Baseline (Stereoscopic [1]) vs. our DepthVanish on attacking RAFT-Stereo [17] and Intel RealSense.

such as limited patch size, varying viewing angles, and dynamic lighting conditions. As illustrated in the first row of Fig. 1, when applied as a physical patch, the Stereoscopic [1] fails to effectively attack RAFT-Stereo and Intel RealSense. This lack of physically realizable and generalizable attack methods presents a significant limitation in evaluating the robustness of stereo systems, particularly as stereo depth estimation continues to be deployed in real-world, safety-critical applications.

In this study, we address these limitations by introducing the first adversarial patch attack that is effective in both digital and physical settings against state-of-the-art (SOTA) deep stereo depth estimation models (Figure 1, second row). Fundamentally, we discover that adding regular intervals between repeated textures shows great potential for improving the attack effectiveness and enables digital-to-physical transferability. Through systematic analysis, we show how interval spacing and texture repetition influence attack success. These insights inform a novel optimization pipeline that jointly designs texture and structure to achieve high attack effectiveness across models and deployment settings. Thus, we propose a novel optimization pipeline that co-designs both texture elements and structural layout for generating adversarial patches that ❶ remain effective when physically printed and inserted into real scenes, ❷ work across diverse datasets and environments and ❸ generalize across different stereo depth estimation models, including commercial RGB-D sensors, *i.e.*, Intel RealSense. In summary, our contributions are as follows,

- We introduce the first adversarial attack that is both digitally and physically effective for deep stereo depth estimation models, including the SOTA RAFT-Stereo and Stereo Transformer.
- Through empirical analysis, we discover that regular interval spacing between repeated textures significantly improves real-world transferability over naive texture repetitions.
- We develop a joint optimization algorithm that co-designs the texture content and spatial structure of the patch to maximize the digital and physical attack effectiveness.
- By physically evaluating our patch, we expose severe safety concerns of existing stereo depth estimation systems and highlight the emergency of practical model robustness enhancement.

2 Related Work

Stereo depth estimation. Stereo-based depth estimation is a technique that infers scene depth from visual correspondences—captured as disparity maps—between pairs of stereo images in various applicable settings [21, 32, 2, 23, 22]. Traditional methods typically follow a multi-stage pipeline involving the computation of matching costs, cost aggregation, and optimization to predict and refine disparities [24]. In contrast, recent advances have incorporated deep neural networks [27], enabling end-to-end learning of feature representations for correspondence matching and direct prediction of disparity and/or depth. In particular, CNN-based methods [4, 12, 31, 36, 20, 25] typically build 3D cost volumes from shared-weight feature encoders, while attention-based models [16, 11, 26, 14] employ vision transformers to model global correspondences and disambiguate difficult regions. Compared to monocular methods [33, 34], stereo offers improved robustness by leveraging geometric constraints from dual viewpoints, but still faces challenges in low-texture and repetitive areas [37, 19].

Depth estimation attack. Thanks to their effectiveness and potential for real-time performance, depth estimation systems have become integral to safety-critical applications such as autonomous driving [6] and robotic navigation [3]. Monocular depth estimation models, in particular, have been extensively studied under both digital [28, 5, 35] and physical adversarial attacks [8, 18, 39, 38]. These evaluations have revealed various system vulnerabilities and led to the development of tailored defense strategies [13, 9, 7], including adversarial training and robust feature learning. In contrast, stereo depth estimation systems—despite their geometric soundness and widespread deployment—have received relatively limited adversarial attention. Existing research has focused primarily on digital, white-

box attacks [1, 29], overlooking potential vulnerabilities in the physical world and leaving a lack of effective defense strategies. This gap is especially concerning given stereo systems’ reliance on precise left-right correspondence, where failures can have serious real-world implications—particularly in autonomous systems that depend on accurate and reliable 3D perception [32].

3 Motivation

3.1 Naive Repetition Fails in Realistic Patch Attacks

Stereo depth estimation recovers 3D structure by identifying correspondences between left and right images, typically formulated as a pixel-wise optimization along epipolar lines:

$$d^*(x) = \arg \min_d C(x, d), \tag{1}$$

where $C(x, d)$ denotes the matching cost between pixel x in the left image and pixel $x - d$ in the right image. When repetitive patterns are presented, the cost volume exhibits periodic ambiguity:

$$C(x, d) \approx C(x, d + ns), \quad \forall n \in \mathbb{Z}, \tag{2}$$

where s denotes the spatial repetition period. This periodicity produces multiple equally plausible matches, thereby increasing the likelihood of incorrect or unstable depth estimations.

Previous adversarial attacks inject repetitive noise over the entire image to exploit periodic ambiguities [1]. Since global noise injection is impractical in real-world scenarios, we instead explore attacks using localized adversarial patches. Nevertheless, simply optimizing repetitive patterns within a patch does not yield effective attacks. As shown by the black curve in Fig. 2(a), simply repeating the pattern within patches results in predicted depth that remains same to the ground truth, indicating limited adversarial effectiveness. This is visually confirmed in Fig. 2(b) (top left), where a naive repeated patch yields a predicted depth of 7.1 m, which is almost identical to the ground truth of 7 m. This observation reveals a key limitation of existing studies: naive repetition fails to generate sufficient ambiguity within small patches, motivating the need for more structured pattern designs.

3.2 Structured Intervals: Enhancing Patch Adversarial Effectiveness

To address this limitation, we propose introducing structured intervals within repeated patterns to effectively amplify stereo matching ambiguity, thereby enhancing the adversarial effect of the patch.

We systematically evaluate the

impact of different interval configurations on the RAFT-Stereo model using the KITTI dataset. As shown in Fig. 2(a) and visualized in Fig. 2(b), structured intervals notably enhance attack effectiveness: ❶ Basic Repeat (black): Depth predictions remain close to the ground truth, indicating minimal adversarial influence. ❷ Horizontal Interval (blue): Moderate overestimation beyond 15 m (*i.e.*, a 20 m true depth yields a ~ 24 m prediction). Visual results (Fig. 2(b), bottom left) confirm a slight increase to 7.2 m. ❸ Vertical Interval (green): Produces larger errors, frequently reaching ~ 30 m at a 20 m ground truth. In Fig. 2(b) (top right), the predicted depth surges to 12.7 m. ❹ Grid Interval (red): Combining both directions produces the strongest adversarial effect, with depth predictions surpassing 40 m at a 23 m ground truth. In the visual result (Fig. 2(b), bottom right), the predicted depth reaches 14.1 m, demonstrating a significant attack impact.

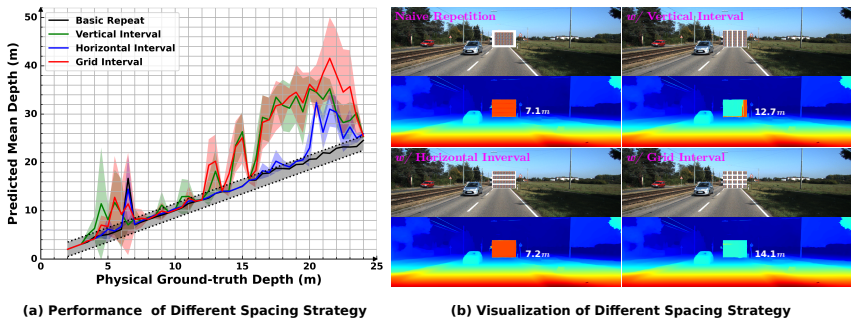


Figure 2: Adversarial effect of interval spacing on depth prediction. (a) Mean predicted depth (solid lines) and variance (shaded regions) for different interval strategies, averaged over interval widths of 2–10 px. The gray dashed band indicates ± 1.5 m from the ground truth. (b) Visualization of typical results where the physical ground truth depth is 7 m.

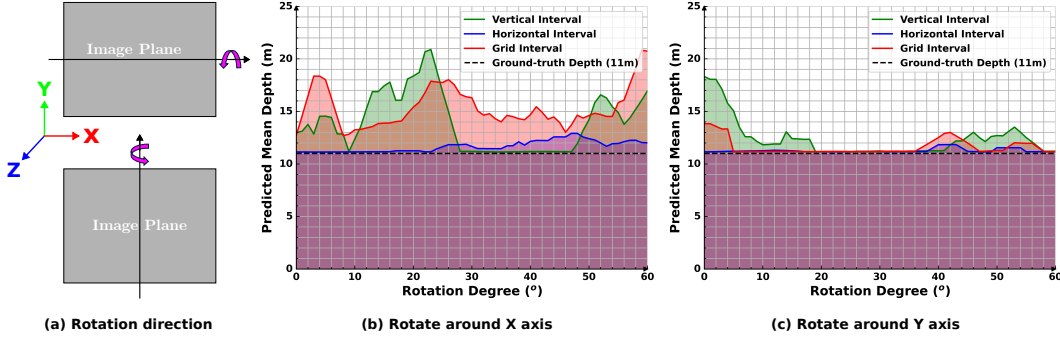


Figure 3: RAFT-Stereo depth prediction performance under various interval structures and patch rotation degrees. (a) Illustration of rotation around the Y and X axes. (b) Depth prediction performance with different rotation degrees around X axis. (c) Depth prediction performance with different rotation degrees around Y axis.

In summary, structuring the patch with both horizontal and vertical intervals (*i.e.*, grid spacing) greatly increases the adversarial effect of patches, far exceeding the impact of simple repetition. However, we also observe two critical limitations: ❶ the overall attack performance remains limited, especially when the patch is placed close to the camera. ❷ the significant variation in performance across different interval configurations suggests that a single fixed interval structure is insufficient.

3.3 Structured Intervals: Improving Attack Robustness across Viewpoints

A practical adversarial patch must maintain its effectiveness even when the patch is rotated or viewed from different orientations. This is particularly important under real-world deployment conditions, where precise placement is difficult to control. To this end, we systematically evaluate the impact of interval structure on attack robustness against patch rotation, as shown in Fig. 3.

For X-axis rotation (Fig. 3(b)): ❶ The horizontal (blue) and vertical (green) intervals exhibit angle-dependent performance, succeeding only at certain angles. ❷ The grid interval (red) is more robust, demonstrating more consistent effectiveness across different angles. For Y-axis rotation (Fig. 3(c)), although all configurations show moderate attack robustness across viewpoints, adding intervals still yields improvements. These results show that structured intervals improve attack robustness to patch rotation, which is essential for reliable adversarial attacks in real-world scenarios.

In summary, the above findings underscore the promise of structured intervals but also reveal their limitations under varying depths and configurations. These observations highlight the need for further optimization of the patch’s texture and structure to achieve more effective attacks.

4 Problem Formulation

To formalize the stereo depth estimation task and define our attack objective, we begin with the following setup. Given a stereo image pair $(\mathbf{I}_l, \mathbf{I}_r)$ and $\mathbf{I} \in \mathbb{R}^{3 \times H \times W}$ of a specific scene, a pretrained stereo depth estimation model $\mathcal{F}(\cdot)$ predicts the pixel-wise disparity map $\mathbf{d}_{pred} = \mathcal{F}(\mathbf{I}_l, \mathbf{I}_r) \in \mathbb{R}^{H \times W}$. The corresponding depth map is computed as $\mathbf{z} = \frac{f \times B}{\mathbf{d}_{pred}}$ where f and B denote the focal length and baseline of the stereo camera rig respectively.

In general, the objective of the attack is to construct an adversarial patch $\mathbf{P} \in \mathbb{R}^{3 \times h_p \times w_p}$ such that the stereo depth estimation model $\mathcal{F}(\cdot)$ produces an incorrect disparity output:

$$\mathcal{F}(\hat{\mathbf{I}}_l, \hat{\mathbf{I}}_r) \neq \mathcal{F}(\mathbf{I}_l, \mathbf{I}_r) \quad (3)$$

where $\hat{\mathbf{I}}_l, \hat{\mathbf{I}}_r$ represent the stereo images with the adversarial patch \mathbf{P} deployed at region p in the original scene. As shown in Sec. 3, interval spacing can trigger critical estimation failures, such as the depth disappearance attack. To demonstrate this vulnerability, we define a stronger attack objective:

$$\mathcal{F}(\hat{\mathbf{I}}_l, \hat{\mathbf{I}}_r) = \mathbf{0}, \quad s.t. \quad \mathbf{d}_{gt}^p = \mathbf{c}, \quad (4)$$

where the model predicts zero disparity for the patch region (*i.e.*, infinite depth), despite the ground truth \mathbf{d}_{gt}^p indicating a fixed, close distance \mathbf{c} . This attack objective reveals more severe vulnerabilities than Eq. (3) and poses substantial safety risks, particularly when the patch is physically realizable and effective in real-world deployments.

5 Methodology

In this work, we build upon our novel findings in Sec. 3 and propose realizing the attack goal in Eq. (4) by exploiting the attack capability of interval spacing. However, this is a non-trivial problem since ❶ Eq. (4) requires the patch’s ground-truth depth to be close but Fig. 2 (a) indicates interval spacing performs weak when the patch is deployed closely. Moreover, ❷ the robustness to rotation is a critical requirement for the patch to be physically attack effective. Yet we observed in Fig. 3 that the robustness provided by the naive interval strategy is rather limited especially for Y axis. It is obvious that an advanced interval spacing strategy is required to realize our attack goal in Eq. (4).

Fundamentally, interval spacing induces a mask \mathbf{M} that partitions the patch \mathbf{P} into interval structure $\mathbf{P}_s = \mathbf{M} \odot \mathbf{P}$ and texture structure $\mathbf{P}_t = (1 - \mathbf{M}) \odot \mathbf{P}$, such that $\mathbf{P} = \mathbf{P}_s + \mathbf{P}_t$. Hence, we propose to optimize these components to reveal their adversarial effects. Since the interval spacing—and thus the mask \mathbf{M} —is predefined (Sec. 3), we focus on optimizing the texture structure \mathbf{P}_t , which consists of tiled texture elements \mathbf{E} , forming the basis of our Grid-based Attack. We then introduce the Depth Vanish Attack, which jointly optimizes both \mathbf{P}_s and \mathbf{P}_t for maximal effect.

5.1 Grid-based Attack

In general, it is straightforward to setup an optimization pipeline for optimizing the texture element with grid intervals, where the patch is formed by repeating the texture elements over the grid. Fundamentally, there two main aspects need to be considered: ❶ the physical constraint required for the texture element to form a patch and ❷ the objective function adopted for optimization.

Given our primary goal is to achieve physical attack effectiveness, the patch must comply with the physical geometry constraints during the optimization. In specific, given a user pre-defined patch physical size (u, v) and physical distance to the camera e in meters, we first find the corresponding pixel size of the patch (h_p, w_p) with the help of stereo calibration information (See details in Sec. 6.1). Then, we empirically apply the optimal interval width o and repetition times k from Sec. 3 to determine the texture element size (h_t, w_t) for \mathbf{E} as,

$$h_t = \frac{h_p - k \cdot o}{k + 1}, \quad w_t = \frac{w_p - k \cdot o}{k + 1}. \quad (5)$$

Based on the size of the texture element, the texture component \mathbf{P}_t —and consequently the full patch \mathbf{P} —is constructed by tiling the base texture unit \mathbf{E} in a regular grid pattern. With the correctly assembled and deployed grid-based patch, we set the optimizing objective function as regional mean square error (rMSE) which is formulated as

$$\mathcal{L}_{rMSE} = \frac{1}{h_p \cdot w_p} \sum_{i=1}^{h_p} \sum_{j=1}^{w_p} (\mathcal{F}(\hat{\mathbf{I}}_l, \hat{\mathbf{I}}_r) - \mathcal{F}(\mathbf{I}_l, \mathbf{I}_r))^2. \quad (6)$$

Let \mathcal{R} be the set of $k \times k$ grid locations on where \mathbf{E} is repeated. The texture element is updated with average gradients: $\mathbf{E} \leftarrow \mathbf{E} - \eta \cdot \frac{1}{|\mathcal{R}|} \sum_{(i,j) \in \mathcal{R}} \nabla_{\mathbf{E}} \mathcal{L}_{rMSE}^{(i,j)}$, where η is the learning rate. Gradients are only applied to the repeated texture regions; the interval areas remain untouched.

5.2 Depth Vanish Attack

As we will see in Fig. 5, the above grid-based optimization can successfully realize attack against various stereo systems but the results are still far from our attack goal defined in Eq. (4). Thus we further consider to optimize the interval structure \mathbf{P}_s at the same time as updating the texture element \mathbf{E} . Practically, optimizing the interval structure on patch level will break the texture repetitions as the interval will be updated to have irregular size. To keep the repetitions and incorporate the interval’s attack capability, we propose to optimize the interval structure within the texture element, *i.e.*, element level, then following [1] repeat the optimized texture element \mathbf{E} forming the final patch.

Same to grid-based attack, given a user pre-defined patch physical size (u, v) and physical distance to the camera e in meters, we first find the corresponding pixel size of the patch (h_p, w_p) . Then we calculate the texture element size (h_t, w_t) by simply dividing (h_p, w_p) to the repetition times k . In order to optimize the texture element so that the interval structure integrated as part of the texture, we propose to regularize the texture element \mathbf{E} during optimization with two objectives. First, we

directly cast entropy constraint on the texture element for regularizing its values to be binary, so that a crisp separation is formed to serve as the required interval structure.

$$\mathcal{L}_{entropy} = \frac{1}{h_t \cdot w_t} \sum_{i=1}^{h_t} \sum_{j=1}^{w_t} -\mathbf{E}_{ij} \log(\mathbf{E}_{ij} + \epsilon) - (1 - \mathbf{E}_{ij}) \log(1 - \mathbf{E}_{ij} + \epsilon), \quad (7)$$

However, we experimentally found that the texture element cannot form a clear pattern with only entropy regularization. As a result, we further integrate the total variation loss to penalizes local pixel-level variation, encouraging the formation of smooth areas.

$$\mathcal{L}_{tv} = \frac{1}{h_t \cdot w_t} \sum_{i=1}^{h_t} \sum_{j=1}^{w_t} |\mathbf{E}_{i+1,j} - \mathbf{E}_{ij}| + |\mathbf{E}_{i,j+1} - \mathbf{E}_{ij}|. \quad (8)$$

With the entropy and total variant constraints, we arrived at an objective function that can shape a clearly interval pattern for the texture element. In summary, the overall objective function adopted for optimization is formulated as

$$\mathcal{L} = \mathcal{L}_{rMSE} + \alpha * \mathcal{L}_{entropy} + \beta * \mathcal{L}_{tv} \quad (9)$$

where α and β are the hyper-parameters balancing the sharp border and coherent region requirements. Hence, we update with, $\mathbf{E} \leftarrow \mathbf{E} - \eta \cdot \frac{1}{|\mathcal{R}|} \sum_{(i,j) \in \mathcal{R}} \nabla_{\mathbf{E}} \mathcal{L}^{(i,j)}$, where η is the learning rate.

5.3 Implementation Details.

During the optimization of grid-based and depth vanish attack, we keep adopt a patch with a physical size $(u, v) = (0.891m, 1.26m)$ and specify the physical ground-truth depth $e = 5m$. To assemble the texture element into patch, we empirically set the repetition as 5 for horizontal and 4 for vertical, *i.e.*, $k = (4, 5)$. For the optimization and corresponding evaluation results with different patch physical setup, we provide them in the supplemental material. When the patch is optimize as grid-based attack, the optimal interval size $o = 10\text{px}$ from Sec. 3 is applied. As for the loss weights adopted during the depth vanish attack, we keep setting $\alpha = 0.1$ and $\beta = 10$. Please find more details of implementation for both grid-based and depth vanish attack in the supplement.

6 Experiments

6.1 Experimental Setup

Dataset. For the evaluation of digital attack effectiveness, we adopt the stereo images from KITTI scene flow (KITTI-scene) [21] and DrivingStereo [32] datasets. Both datasets composed of stereo images for urban traffic scenes where the image size of KITTI-scene is (1242,375) and DrivingStereo is (1758, 800). In more detail, we adopt the four sub-sets of DrivingStereo that captured under different weather conditions (*i.e.*, sunny, foggy, rainy, cloudy) where we report the attack performance for each of them respectively. Following [1], 40 stereo image pairs for each (sub-)dataset are selected to verify the effectiveness of different patches. For the physical evaluation, we manually capture stereo images with i3DStreoid² where various safety critical situations are considered. We refer readers to the supplemental material for the details of how the physical stereo images are captured and the pipeline we adopted for physical deployment.

Attack targets. Following [29, 1], we apply our attack method to PSMNet [4], DeepPruner [10] and AANet [30] for validating the general attack effectiveness. Moreover, we empirically found that they are out-of-date and easily to be disturbed, thus we further select RAFT-Stereo [17] and STereo TRansformer (STTR) [15] which represents the most promising iterative optimization-based methods and transformer-base methods as our main attack targets. For the detail hyper-parameter setting and the pretrained checkpoint adopted during the attack, please find all of them in supplemental material.

²<http://stereo.jpn.org/eng/iphone/help/index.html>

Digital deployment. During the digital optimization and evaluation, the patch needs to be placed inside the scene following the physical constraints. To achieve this, we apply the calibration information provided by the KITTI and DrivingStereo dataset. In specific, given a patch with predefined physical size in meters, we first set the homogeneous 3D position of the patch’s corners regarding to the reference camera coordinate system. Then we calculate the corresponding pixel coordinates with the help of the rectified projection and rotation matrix. The full calculation is detailed in supplement.

Table 1: Statistical attack performance of our DepthVanish, grid-based patch and existing baselines for PSMNet, DeepPruner, AANet, RAFT-Stereo and STTR on KITTI-scene dataset. The best results are highlighted in **bold**.

KITTI-scene	PSMNet		DeepPruner		AANet		RAFT-Stereo		STTR	
	D1	EPE	D1	EPE	D1	EPE	D1	EPE	D1	EPE
Stereoscopic Patch	6.23 \pm 1.13	5.28 \pm 0.88	8.29 \pm 10.23	3.29 \pm 2.05	6.79 \pm 2.30	3.69 \pm 0.39	5.79 \pm 9.88	3.58 \pm 6.73	4.58 \pm 2.83	1.30 \pm 5.37
Stereopagnosia Patch	2.17 \pm 0.09	2.18 \pm 0.58	5.40 \pm 11.16	1.62 \pm 2.33	3.42 \pm 2.59	1.96 \pm 0.44	4.18 \pm 11.27	2.09 \pm 12.66	3.02 \pm 3.00	1.28 \pm 8.79
Grid-based Patch (ours)	3.35 \pm 1.09	48.21 \pm 8.24	55.39 \pm 10.77	38.60 \pm 3.03	60.59 \pm 8.90	53.84 \pm 4.93	40.09 \pm 5.87	67.24 \pm 7.90	5.23 \pm 7.49	45.34 \pm 7.30
DepthVanish (ours)	55.30 \pm 6.85	50.71 \pm 9.71	97.07 \pm 12.42	67.19 \pm 4.85	66.42 \pm 10.10	56.54 \pm 5.26	89.31 \pm 6.56	66.01 \pm 6.18	92.38 \pm 8.76	69.25 \pm 6.62

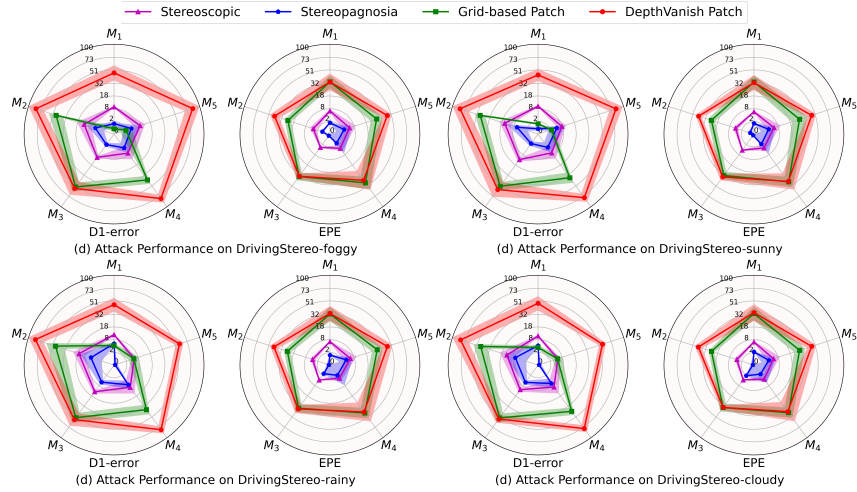


Figure 4: Attack performance of our DepthVanish, grid-based patch and existing baselines for PSMNet (M1), DeepPruner (M2), AANet (M3), RAFT-Stereo (M4) and STTR (M5) on the sub-sets of DrivingStereo dataset.

Evaluation metrics. Following the convention, we adopt bad pixel error (D1-error) and End-Point Error (EPE) for evaluating the prediction performance and they are specifically calculated as

$$D1 = \frac{\# \text{ of bad pixels}}{\# \text{ of total pixels}} \times 100\%, \quad EPE = \frac{1}{N} \sum_{i=1}^N |\mathbf{d}_{pred}^i - \mathbf{d}_{gt}^i|, \quad (10)$$

where the bad pixel is one that satisfy $|\mathbf{d}_{pred} - \mathbf{d}_{gt}| > \max(3, 0.05 \cdot \mathbf{d}_{gt})$. To evaluate patch attack effectiveness, we first follow Eq. (4) to set the ground-truth disparity of the patch as $\mathbf{d}_{gt} = \mathbf{c}$. Then, we define the bad pixels as those satisfying $|\mathbf{d}_{pred} - \mathbf{c}| > \max(3, 0.05 \cdot \mathbf{d}_{gt})$ and $|\mathbf{d}_{pred} - \mathbf{0}| < \frac{\mathbf{c}}{k}$, where k defines how many times deeper than the actual depth will a patch be considered to be attack effective. In summary, we report the average D1-error and EPE with standard deviation where higher values indicate better attack performance.

6.2 Digitally Attack Stereo Estimator

We first conduct digital attack experiments with our proposed DepthVanish patch on KITTI-scene dataset and the four sub-sets of DrivingStereo, *i.e.*, sunny, foggy, rainy, cloudy.

Setting: Due to the lack of existing works on attacking stereo matching with patch, we apply the results from existing digital attack studies (*i.e.*, Stereoscopic [1] and Stereopagnosia [29]) as patches and deploy them into the scene as the first set of baselines. However, it should be noted that such comparison is not fair enough as existing works [1, 29] are not specifically designed for patch attack. Thus we further setup our own baseline (*i.e.*, grid-based patch from Sec. 5.1) for a fair comparison.

Results: **1** We report the attack results for the five attack target models on KITTI-scene dataset in Tab. 1. It can be seen that existing digital attacks are ineffective under the patch attack setup, while

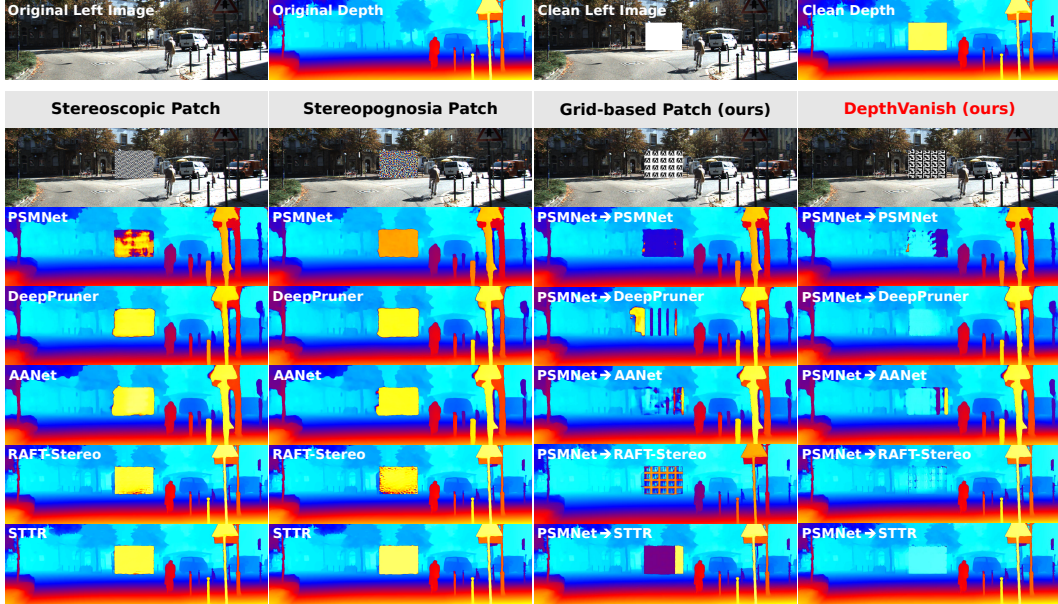


Figure 5: Visualization of different digital patch attack baselines and our DepthVanish patch against different target models on KITTI-scene dataset. Note that the original and clean depth are estimated by RAFT-Stereo.

our Grid-based Patch significantly outperforms them. Notably, DepthVanish achieves strong attack performance, especially against DeepPruner, RAFT-Stereo and STTR. We illustrate the results on DrivingStereo dataset in Fig. 4. It is obvious that similar attack performance can be observed on all the four sub-sets. ② In addition to the standard evaluation, Fig. 5 shows a KITTI sample comparison. Compared to the Clean Depth, we first note that existing attack works fail to mislead all the five target models, where only the Stereoscopic Patch shows slightly influence on PSMNet. However, as the results shown in the last column our DepthVanish patch can cast strong influence where the patch almost disappear. More surprisingly, our patch enjoys significant transferability over models where the patch optimized with PSMNet shows strong attack effect on other four models. From our experimental experience, all the patches with such clear interval patterns are model transferable for which we credit such capability to the insights we analyzed in Sec. 3. Please refer to the supplemental material for the comprehensive experimental results of attack transferability.

6.3 Physically Attack Stereo Estimator

In this section, we conduct physical evaluation for our DepthVanish patches that optimized with different stereo estimators to highlight the importance and emergency of research on stereo matching reliability.

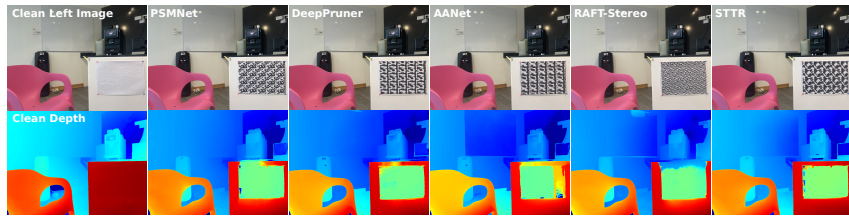


Figure 6: Visualization of physical attack results of our DepthVanish patches against different stereo depth estimators. Note that the clean depth is estimated with RAFT-Stereo.

As shown in Fig. 6, we host our DepthVanish patches on a white board for the purpose of contrasting the depth disturbance. ① It can be observed from the results that our DepthVanish patch consistently preserves its attack effectiveness after deployed into the physical environment. Compared to the Clean Depth, the board region occupied by our DepthVanish patches are predicted as far away in general. ② However, it should be noted that the induced depth error are limited compared to the digital effectiveness in Fig. 5. We ascribe such performance degradation to the lighting variation and imprecise photo capturing process, where the left and right images are captured manually in separate. Therefore, we further conduct evaluation for our patch against commercial stereo depth camera in the next. In summary, despite of the imprecise stereo image capturing process, our DepthVanish attack still keeps successfully attacking SOTA DNN-based stereo depth estimation models with consistency.

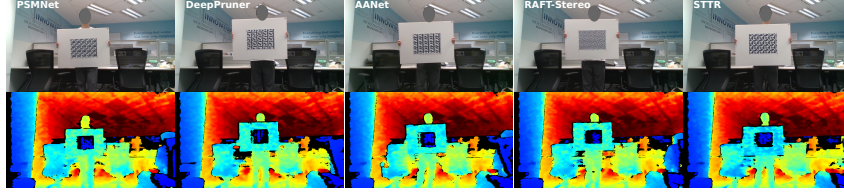


Figure 7: Visualization of DepthVanish attack performance against Intel RealSense depth camera (D435i).

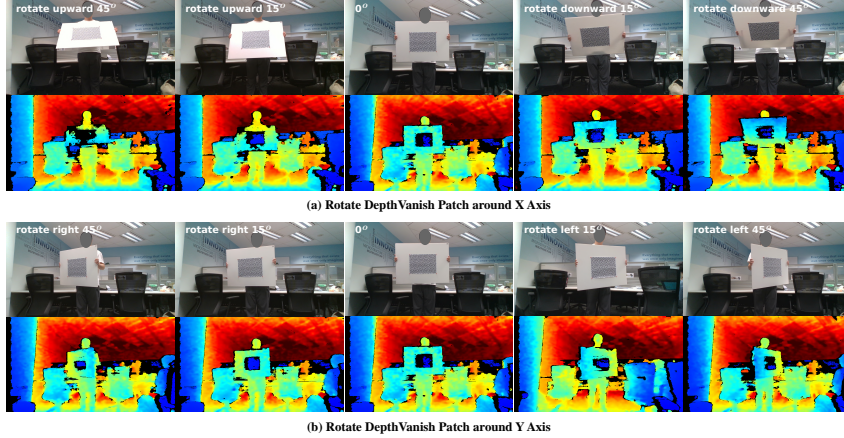


Figure 8: Visualization of DepthVanish attack performance with different rotation degrees around both X and Y axes against Intel RealSense depth camera (D435i).

6.4 Attack Commercial Stereo System

To further assess the practicality and robustness of our DepthVanish patch, we evaluate its performance on a commercial stereo camera system, specifically the Intel RealSense D435i depth camera. We focus on evaluating the patch’s robustness from three aspects: model generalization, geometric transformation, and distance variation. **① Model generalization:** we deploy the patch, optimized on the KITTI dataset, against five stereo models without any extra adaptation. As shown in Fig. 7, the patch consistently disrupts depth predictions across all models, demonstrating strong cross-model transferability. **② Geometric robustness:** we physically rotate the patch along the X and Y axes. As visualized in Fig. 8, the patch remains effective under different viewing angles, confirming its robustness to rotation. **③ Distance robustness:** our method also shows robustness under varying distances. Corresponding visual results are provided in the supplementary material.

6.5 Ablation Study

In this section, we conduct ablation analysis on the DepthVanish attack to assess the impact of the hyperparameters α and β in the objective function (Eq. (9)). As shown in Fig. 9, both parameters are critical for optimal attack performance. Specifically, it can be seen that the performance degraded significantly when $\alpha = 0$, *i.e.*, the $\mathcal{L}_{entropy}$ is removed from Eq. (9), which highlights the importance of the clear interval for attack effectiveness. Moreover, the total variation constraint \mathcal{L}_{tv} is also important where a clear performance degradation can be observed when β decreases below 9. In summary, the collaboration of entropy and total variation regularizations effectively enables our DepthVanish patch to achieve the superior attack performance.

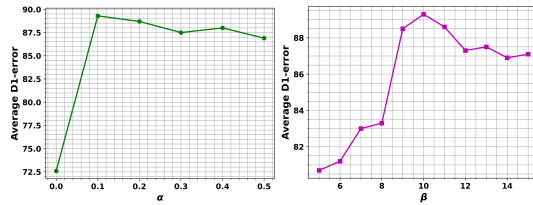


Figure 9: Attack performance of RAFT-Stereo under different α and β . Evaluated on KITTI dataset.

7 Conclusion

In this work, we present DepthVanish, a significant advancement of an adversarial patch attack that jointly optimizes texture and interval structure to target stereo depth systems. By thoroughly

analyzing the effect of interval spacing over repeated texture elements, we provide a novel insight for boosting the attack effectiveness on traditional repeated texture. Unlike previous approaches limited to digital environments, our method effectively “disappears” objects in both digital and physical settings when tested against state-of-the-art models and commercial RGB-D cameras. These findings expose critical vulnerabilities in current depth estimation technologies, highlighting the urgent need for robust defenses in safety-critical autonomous systems.

References

- [1] Zachary Berger, Parth Agrawal, Tian Yu Liu, Stefano Soatto, and Alex Wong. Stereoscopic universal perturbations across different architectures and datasets. In *Proceedings of the IEEE/CVF Conference on Computer Vision and Pattern Recognition*, pages 15180–15190, 2022.
- [2] Johann Cabon, Naila Murray, and Martin Humenberger. Virtual KITTI 2. *CoRR*, abs/2001.10773, 2020.
- [3] Wenxiao Cai, Yaroslav Ponomarenko, Jianhao Yuan, Xiaoqi Li, Wankou Yang, Hao Dong, and Bo Zhao. Spatialbot: Precise spatial understanding with vision language models. *arXiv preprint arXiv:2406.13642*, 2024.
- [4] Jia-Ren Chang and Yong-Sheng Chen. Pyramid stereo matching network. In *Proceedings of the IEEE/CVF Conference on Computer Vision and Pattern Recognition (CVPR)*, 2018.
- [5] Hemang Chawla, Arnav Varma, Elahe Arani, and Bahram Zonooz. Adversarial attacks on monocular pose estimation. In *2022 IEEE/RSJ International Conference on Intelligent Robots and Systems (IROS)*, pages 12500–12505. IEEE, 2022.
- [6] Junda Cheng, Wei Yin, Kaixuan Wang, Xiaozhi Chen, Shijie Wang, and Xin Yang. Adaptive fusion of single-view and multi-view depth for autonomous driving. In *Proceedings of the IEEE/CVF Conference on Computer Vision and Pattern Recognition (CVPR)*, pages 10138–10147, June 2024.
- [7] Zhiyuan Cheng, Cheng Han, James Liang, Qifan Wang, Xiangyu Zhang, and Dongfang Liu. Self-supervised adversarial training of monocular depth estimation against physical-world attacks. *IEEE Transactions on Pattern Analysis and Machine Intelligence*, 46(12):9084–9101, 2024.
- [8] Zhiyuan Cheng, James Liang, Hongjun Choi, Guan hong Tao, Zhiwen Cao, Dongfang Liu, and Xiangyu Zhang. Physical attack on monocular depth estimation with optimal adversarial patches. In *European Conference on Computer Vision (ECCV)*, 2022.
- [9] Zhiyuan Cheng, James Liang, Guan hong Tao, Dongfang Liu, and Xiangyu Zhang. Adversarial training of self-supervised monocular depth estimation against physical-world attacks. In *The Eleventh International Conference on Learning Representations, (ICLR)*, 2023.
- [10] Shivam Duggal, Shenlong Wang, Wei-Chiu Ma, Rui Hu, and Raquel Urtasun. Deeppruner: Learning efficient stereo matching via differentiable patchmatch. In *Proceedings of the IEEE/CVF international conference on computer vision*, pages 4384–4393, 2019.
- [11] Weiyu Guo, Zhaoshuo Li, Yongkui Yang, Zheng Wang, Russell H. Taylor, Mathias Unberath, Alan L. Yuille, and Yingwei Li. Context-enhanced stereo transformer. In *European Conference on Computer Vision (ECCV)*, 2022.
- [12] Xiaoyang Guo, Kai Yang, Wukui Yang, Xiaogang Wang, and Hongsheng Li. Group-wise correlation stereo network. In *Proceedings of the IEEE/CVF Conference on Computer Vision and Pattern Recognition (CVPR)*, 2019.
- [13] Junjie Hu and Takayuki Okatani. Analysis of deep networks for monocular depth estimation through adversarial attacks with proposal of a defense method. *arXiv preprint arXiv:1911.08790*, 2019.
- [14] Nikita Karaev, Ignacio Rocco, Benjamin Graham, Natalia Neverova, Andrea Vedaldi, and Christian Rupprecht. Dynamicstereo: Consistent dynamic depth from stereo videos. In *Proceedings of the IEEE/CVF Conference on Computer Vision and Pattern Recognition (CVPR)*, 2023.
- [15] Zhaoshuo Li, Xingtong Liu, Nathan Drenkow, Andy Ding, Francis X Creighton, Russell H Taylor, and Mathias Unberath. Revisiting stereo depth estimation from a sequence-to-sequence perspective with transformers. In *Proceedings of the IEEE/CVF international conference on computer vision*, pages 6197–6206, 2021.

- [16] Zhaoshuo Li, Xingtong Liu, Nathan Drenkow, Andy S. Ding, Francis X. Creighton, Russell H. Taylor, and Mathias Unberath. Revisiting stereo depth estimation from a sequence-to-sequence perspective with transformers. In *Proceedings of the IEEE/CVF International Conference on Computer Vision (ICCV)*, 2021.
- [17] Lahav Lipson, Zachary Teed, and Jia Deng. Raft-stereo: Multilevel recurrent field transforms for stereo matching. In *2021 International Conference on 3D Vision (3DV)*, pages 218–227. IEEE, 2021.
- [18] Hangcheng Liu, Zhenhu Wu, Hao Wang, Xingshuo Han, Shangwei Guo, Tao Xiang, and Tianwei Zhang. Beware of road markings: A new adversarial patch attack to monocular depth estimation. In *Advances in Neural Information Processing Systems (NeurIPS)*, 2024.
- [19] Baoli Lu, Liang Sun, Lina Yu, and Xiaoli Dong. An improved graph cut algorithm in stereo matching. *Displays*, 2021.
- [20] Yamin Mao, Zhihua Liu, Weiming Li, Yuchao Dai, Qiang Wang, Yun-Tae Kim, and Hong-Seok Lee. Uasnet: Uncertainty adaptive sampling network for deep stereo matching. In *Proceedings of the IEEE/CVF International Conference on Computer Vision (ICCV)*, 2021.
- [21] Moritz Menze, Christian Heipke, and Andreas Geiger. Object scene flow. *ISPRS Journal of Photogrammetry and Remote Sensing (JPRS)*, 2018.
- [22] Pierluigi Zama Ramirez, Fabio Tosi, Matteo Poggi, Samuele Salti, Stefano Mattocchia, and Luigi Di Stefano. Open challenges in deep stereo: the booster dataset. In *Proceedings of the IEEE/CVF Conference on Computer Vision and Pattern Recognition*, 2022.
- [23] Daniel Scharstein, Heiko Hirschmüller, York Kitajima, Greg Krathwohl, Nera Nestic, Xi Wang, and Porter Westling. High-resolution stereo datasets with subpixel-accurate ground truth. In *Proceedings of German Conference on Pattern Recognition*, 2014.
- [24] Daniel Scharstein and Richard Szeliski. A taxonomy and evaluation of dense two-frame stereo correspondence algorithms. *International Journal of Computer Vision*, 47(1-3):7–42, 2002.
- [25] Zhelun Shen, Yuchao Dai, Xibin Song, Zhibo Rao, Dingfu Zhou, and Liangjun Zhang. Pcw-net: Pyramid combination and warping cost volume for stereo matching. In *European Conference on Computer Vision (ECCV)*, 2022.
- [26] Qing Su and Shihao Ji. Chitransformer: Towards reliable stereo from cues. In *Proceedings of the IEEE/CVF Conference on Computer Vision and Pattern Recognition (CVPR)*, 2022.
- [27] Fabio Tosi, Luca Bartolomei, and Matteo Poggi. A survey on deep stereo matching in the twenties. *International Journal of Computer Vision*, 2025.
- [28] Alex Wong, Safa Cicek, and Stefano Soatto. Targeted adversarial perturbations for monocular depth prediction. *Advances in neural information processing systems*, 33:8486–8497, 2020.
- [29] Alex Wong, Mukund Mundhra, and Stefano Soatto. Stereopagnosia: Fooling stereo networks with adversarial perturbations. In *Proceedings of the AAAI Conference on Artificial Intelligence*, volume 35, pages 2879–2888, 2021.
- [30] Haofei Xu and Juyong Zhang. Aanet: Adaptive aggregation network for efficient stereo matching. In *Proceedings of the IEEE/CVF conference on computer vision and pattern recognition*, pages 1959–1968, 2020.
- [31] Gengshan Yang, Joshua Manela, Michael Happold, and Deva Ramanan. Hierarchical deep stereo matching on high-resolution images. In *Proceedings of the IEEE/CVF Conference on Computer Vision and Pattern Recognition*, pages 5515–5524, 2019.
- [32] Guorun Yang, Xiao Song, Chaoqin Huang, Zhidong Deng, Jianping Shi, and Bolei Zhou. Drivingstereo: A large-scale dataset for stereo matching in autonomous driving scenarios. In *IEEE Conference on Computer Vision and Pattern Recognition (CVPR)*, 2019.
- [33] Lihe Yang, Bingyi Kang, Zilong Huang, Xiaogang Xu, Jiashi Feng, and Hengshuang Zhao. Depth anything: Unleashing the power of large-scale unlabeled data. In *CVPR*, 2024.
- [34] Lihe Yang, Bingyi Kang, Zilong Huang, Zhen Zhao, Xiaogang Xu, Jiashi Feng, and Hengshuang Zhao. Depth anything V2. In *Advances in Neural Information Processing Systems (NeurIPS)*, 2024.

- [35] Gyungeun Yun, Kyungho Joo, Wonsuk Choi, and Dong Hoon Lee. Poster: Unveiling the impact of patch placement: Adversarial patch attacks on monocular depth estimation. In *Proceedings of the 2023 ACM SIGSAC Conference on Computer and Communications Security, CCS*, 2023.
- [36] Feihu Zhang, Victor Adrian Prisacariu, Ruigang Yang, and Philip H. S. Torr. Ga-net: Guided aggregation net for end-to-end stereo matching. In *Proceedings of the IEEE/CVF Conference on Computer Vision and Pattern Recognition (CVPR)*, 2019.
- [37] Tong Zhao, Mingyu Ding, Wei Zhan, Masayoshi Tomizuka, and Yintao Wei. Depth-aware volume attention for texture-less stereo matching, 2024.
- [38] Junhao Zheng, Chenhao Lin, Jiahao Sun, Zhengyu Zhao, Qian Li, and Chao Shen. Physical 3d adversarial attacks against monocular depth estimation in autonomous driving. In *Proceedings of the IEEE/CVF Conference on Computer Vision and Pattern Recognition, (CVPR)*, 2024.
- [39] Tianyue Zheng, Jingzhi Hu, Rui Tan, Yinqian Zhang, Ying He, and Jun Luo. pi-jack: Physical-world adversarial attack on monocular depth estimation with perspective hijacking. In *33rd USENIX Security Symposium, USENIX Security*, 2024.

A Experimental Environment

All of the experiments are conducted on a server with AMD EPYC 9554 64-core Processor and an NVIDIA L40 GPU, running Ubuntu 22.04. During the physical evaluation, the patch is first printed out with an EPSON L18050 printer, *e.g.*, a patch of physical size $(u, v) = (0.891m, 1.26m)$ is printed out by filling A3 size paper.

B Implementation Details

B.1 Calculation for Digital Deployment

During the digital experiments, the patches are first digitally deployed into the scene. As our aim is to achieve physical attack, it requires the digital deployment follows the physical constraints. Fortunately, such physical-constraint digital patch deployment can be realized with the calibration information provided by the dataset. We show the detail calculation for KITTI dataset in the follow.

For KITTI dataset, we suppose the patch’s physical size and depth are predefined with regard to the camera 0 (the reference camera). Given the patch with physical size of (w_p, h_p) , we intend to deploy it into a KITTI scene with physical depth e .

1. Get the corresponding calibration information for the scene from ‘calib_cam_to_cam’ folder provided by KITTI scene flow dataset.
2. Retrieve the three rectified calibration matrix $P_{rect_02}, P_{rect_03}, R_{rect_00}$.
3. Specify the physical shifting (x_{shift}, y_{shift}) (in meters) of the patch center with regard to the camera 0 principal axis.
4. Set the homogeneous coordinates for the corners of the patch as:
 - $top_left = (-w_p/2 + x_{shift}, -h_p/2 + y_{shift}, e, 1)$,
 - $top_right = (w_p/2 + x_{shift}, -h_p/2 + y_{shift}, e, 1)$,
 - $bottom_left = (-w_p/2 + x_{shift}, h_p/2 + y_{shift}, e, 1)$,
 - $bottom_right = (w_p/2 + x_{shift}, h_p/2 + y_{shift}, e, 1)$.
5. For the pixel coordinates of the patch’s corner in the right stereo image, get them with $(P_{rect_02} \times R_{rect_00}) \cdot c$ where c is the corners homogeneous coordinates.
6. Similarly, get the corresponding pixel coordinates for the left stereo image with $(P_{rect_03} \times R_{rect_00}) \cdot c$.
7. Finally, the patch is deployed into the scene by applying perspective transformation to fit the patch into the calculated pixel region.

For the calculation of DrivingStereo, the process is the same as KITTI except for the reference camera is camera 1 thus $P_{rect_101}, P_{rect_103}$ and R_{rect_101} from their calibration file is adopted.

B.2 Physical Stereo Image Capture

During the experiments of physical evaluation of our patch, we have to manually capture the scene due to the lack of RGB stereo capturing device. We adopt the i3DSteroid mobile application which is specifically designed to facilitate the capturing of stereo images with mobile phone of model iPhone 14 pro. In specific, a cutting board of A3 size is utilized to place the mobile phone for a 30cm baseline simulation. Then at each place a picture is taken by the mobile phone as one of the stereo image. However, we do aware the inaccuracy of such stereo image capturing process that is also we further test our patch with commercial RGB-D camera, *i.e.*, IntelRealSense D435i.



Figure 1: Illustration of i3DSteroid.

B.3 Setting for Attack Targets

For the PSMNet, DeepPruner and AANet, we follow the setup of Stereoscopic [1] and directly adopt the API provided at <https://github.com/alexklwong/stereoscopic-universal-perturbations.git>. As for the RAFT-Stereo and STTR, we use the official code release and integrate them following Stereoscopic code. And the checkpoint pretrained on KITTI dataset for both models, *i.e.*, ‘raftstereo-sceneflow.pth’ and ‘kitti_finetuned_model.pth.tar’, are adopt for experiments. Note that we keep setting $k = 3$ for D1-error metric calculation during the evaluation for all the attack target models.

C Experimental Results

C.1 Optimize under Different Setup

We conduct experiments to test the influence of the patch physical size and depth. As shown in Fig. 2, we test physical depth ranges from $5m$ to $21m$ and different physical size by setting the patch as a scaled size of $(0.891m, 1.26m)$. In general, we see the patch keeps be attack effective across different physical size and depth. Empirically, a patch will show great disturbance when the D1-error larger than 80 which physically represents an disappeared object for the stereo system.

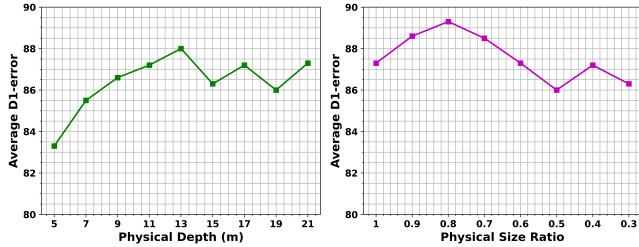


Figure 2: Attack performance of the our DepthVanish patch with different patch physical size and depth.

C.2 Attack Transferability Results

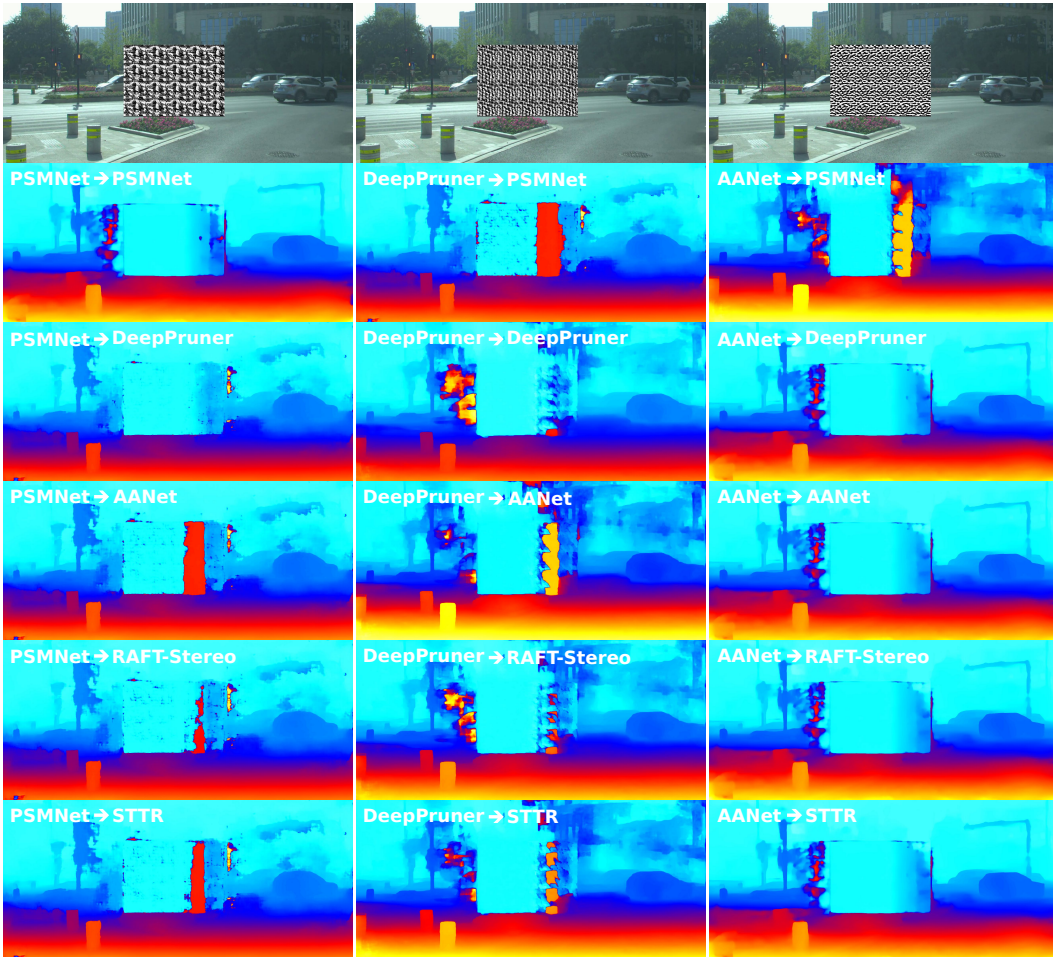


Figure 3: Visualization of attack transferability results of our DepthVanish patches against different stereo depth estimators on KITTI scene.

As we have show our DepthVanish patch enjoys strong attack transferability over different stereo estimation models, we further visualize such merit in Fig. 3 and Fig. 4 on KITTI and DrivingStereo dataset respectively. Although it can be seen that there are some unsatisfying results on KITTI dataset, we can observe our DepthValish patch keeps successfully attacking all the models with different transferability.

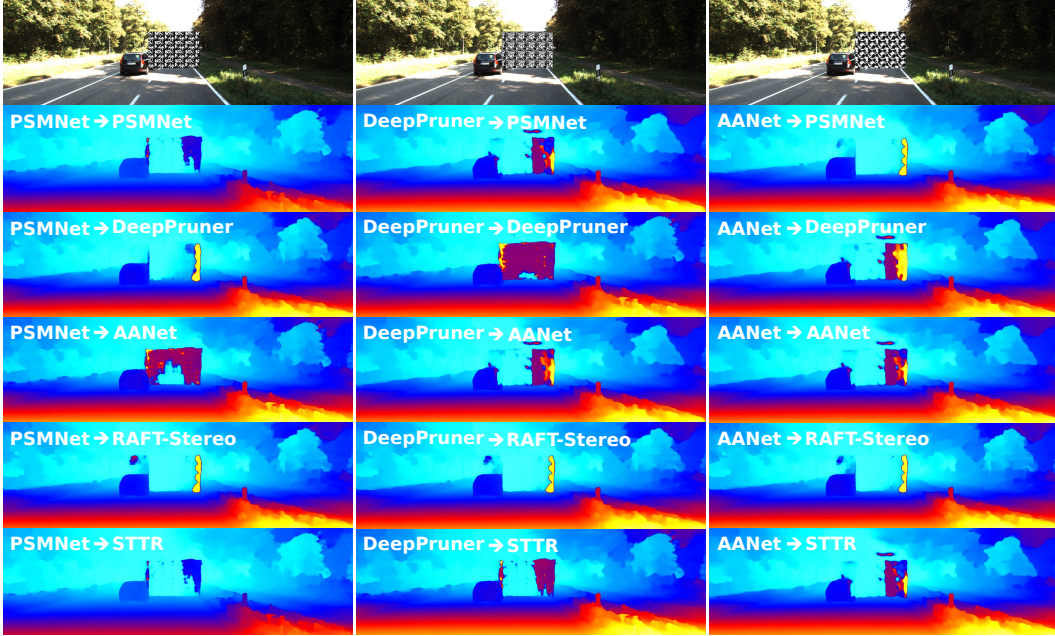


Figure 4: Visualization of attack transferability results of our DepthVanish patches against different stereo depth estimators on DrivingStereo scene.

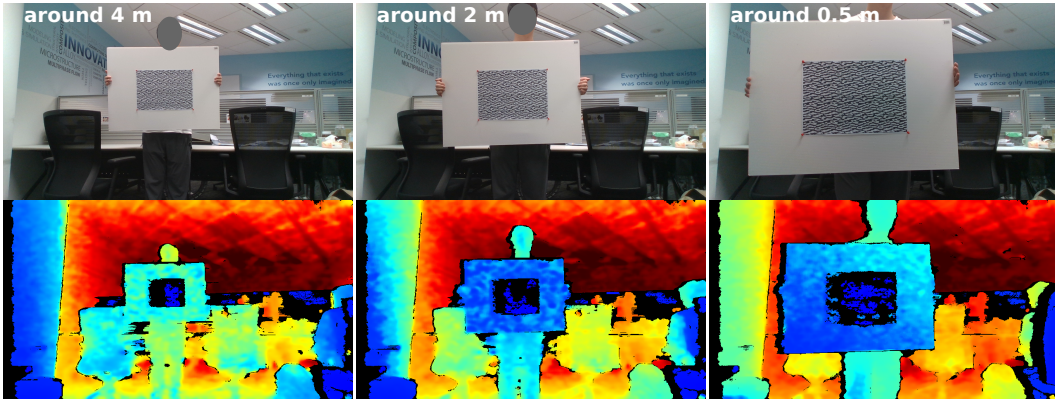


Figure 5: Visualization of our DepthVanish patch's robustness across different distance.

C.3 Distance Robustness

As we have verified the rotation robustness of our patch in the main experiments, here we further show our DepthVanish patch is also robust to distance. As shown in Fig. 5, our DepthVanish patch (optimized with RAFT-Stereo) remains attack effective with the variation of distance.

D Limitation

Our research has several important limitations regarding the attack methodology. Due to limited testing scope, we cannot guarantee the robustness of our attack methods against the full spectrum of existing DNN architectures for stereo depth estimation. Additionally, we have not evaluated our attacks against existing robustified methods or defense mechanisms that may be implemented in real-world systems, which may overestimate the practical effectiveness of the vulnerabilities we identified. Regarding defensive approaches, our work lacks comprehensive solutions to the vulnerabilities demonstrated. While we discussed several potential defense strategies in the next section, we do not provide thoroughly tested, reliable defense methods with rigorous evaluation of their effectiveness or practical implementability. Furthermore, we have not explored the deeper theoretical principles underlying these vulnerabilities, limiting the ability to provide principled guidance for designing inherently robust depth estimation systems.

E Broader Impact

Scientific & Societal Benefit In conducting our research on digital and physical attacks against stereo depth estimation models, we identify several important benefits to the scientific community and society. ❶ Through our identification of vulnerabilities in current depth estimation algorithms, we highlight critical weaknesses that need addressing before these systems are widely deployed in safety-critical applications. By revealing these issues in a controlled research setting, we enable improvements before real-world failures occur. ❷ Our work advances fundamental understanding of robustness in computer vision systems, particularly for depth perception, which is essential for autonomous vehicles, robotics, augmented reality, and medical imaging systems. This knowledge can lead to more resilient algorithms and implementations. ❸ Our physical attack demonstrations help bridge the gap between theoretical and practical security concerns, providing empirical evidence that can drive industry standards and testing protocols for vision-based systems before deployment.

Misuse Potential & Security Concern We acknowledge there are legitimate concerns about how this research could be misused, thus we carefully considered the ethical implications of revealing vulnerabilities in stereo depth estimation systems. Malicious actors might exploit the vulnerabilities we have identified to compromise autonomous navigation systems in vehicles or robots, potentially causing accidents or enabling theft/tampering of autonomous systems. As a result, we implemented several safety controls to minimize misuse risk, including: ❶ limited disclosure of specific technical details that could enable immediate exploitation; ❷ establishment of a reasonable timeline for patches before full disclosure; ❸ creation of a centralized database of proposed attacks accessible only to verified researchers and industry partners We recommend similar safeguards for related research, including mandatory ethics review for attack demonstrations, implementation of differential privacy techniques to limit what information is shared, developing standardized responsible disclosure protocols specific to vision system vulnerabilities. By maintaining these ethical standards and safety controls, we can continue advancing security research while minimizing potential harm to systems that increasingly underpin critical infrastructure and everyday technologies.

Possible Defense Based on our findings, we propose several potential defensive approaches that could help mitigate the vulnerabilities our research identifies. ❶ Ensemble approaches that combine multiple depth estimation techniques (e.g., stereo, monocular, LiDAR fusion) can reduce the effectiveness of attacks targeted at any single method. ❷ Adversarial training with examples similar to our attack vectors could significantly improve model robustness, especially if incorporating both digital and physical attack factors. ❸ Runtime anomaly detection systems that identify sudden or physically implausible changes in depth maps could flag potential attacks for secondary verification. Other possible direction includes physical hardening through careful sensor placement, multi-angle verification, and environmental controls could reduce the effectiveness of physical attacks in critical systems. We suggest regulatory frameworks requiring security testing against known attack vectors like those we have identified could help ensure systems meet minimum safety standards before deployment.